

# Development of a 3D Printed Multi-Axial Force Sensor

Qinglei JI<sup>a,b</sup> Shuo FU<sup>b</sup> Lei FENG<sup>b</sup> Georgios ANDRIKOPOULOS<sup>b</sup>  
Xi Vincent WANG<sup>a</sup> and Lihui WANG<sup>a,1</sup>

<sup>a</sup>*Department of Production Engineering, KTH Royal Institute of Technology, Stockholm 10044, Sweden*

<sup>b</sup>*Department of Machine Design, KTH Royal Institute of Technology, Stockholm 10044, Sweden*

**Abstract.** Sensors play a vital role in the industry transformation. Commercial sensors such as force sensors have limited options in shapes, stiffness, measuring ranges, etc. Customized force sensors optimized for the production environment can greatly increase the integration workflow and avoid the trade-off in design freedom of using commercial sensors. 3D printing, as a rapid prototyping technology, offers great potential in fabricating force sensors customized to a specific application. However, most of the existing 3D printed force sensors are limited to one-directional sensing, while most of them use materials developed in-house. In this study, a fully 3D printed force sensor using commercial conductive 3D printing materials is presented. By utilizing the resistance change when under load, the sensor can estimate the applied force in multiple directions. The resistive performance of the prototype 3D printed force sensor is first characterized and then validated in a case study.

**Keywords.** Multi-axial sensor, force sensor, 3D printing, modeling

## 1. Introduction

Sensors are widely applied in modern production lines [1–4]. For example, photoelectric [5] or inductive [6] sensors are used for proximity detection. Temperature sensors are applied for measuring the temperature status of the environment, the machines or the products [7, 8]. Level sensors and vibration sensors can be used to ensure the appropriate working conditions for the machine tools [9]. Speed sensors can be used to control the transmission velocity of the production lines [10, 11]. Computer vision sensors can be used to detect actions, positions or defects using the image sequences captured from the cameras [12].

Among all sensors types, pressure or forces sensors (called as force sensors for simplicity in later context) are one of the most commonly seen sensors, which are employed to measure the pressure or force applied to the target object. These sensors can be integrated onto e.g. robot arms for providing force feedback and perform accurate force control [13]. They can also be used for haptic feedback, to enable precise grasping tasks via

---

<sup>1</sup>Corresponding Author: Lihui WANG, e-mail:lihuiw@kth.se.

grippers with well controlled operation force [14]. Most of these force sensors are strain resistive. When the external force or pressure are applied onto the sensors, they deform and the electric resistance changes accordingly. By measuring the resistance changes and pre-calibrating the sensors, the external forces or pressures can thus be estimated.

Both rigid and flexible force sensors are commercially available. Flexible sensors can sustain much larger stretching or bending deformation than rigid sensors. However, these commercial sensors are mostly provided in fixed or limited sizes and shapes. To select the right sensor to integrate and use for a particular application setup, users have to well characterize the required ranges of measuring, as well as the space requirements for proper sensor placement. When suitable sensors cannot be found for a particular use case, the original design of the target object to be measured has to be modified to fit the requirement of sensor placement and integration, which greatly restricts the product design workflow.

In recent years, researchers from the field of rapid manufacturing started to utilize 3D printing for the fabrication of customized sensors optimized for specific application scenarios. 3D printing technologies produce objects by on-demand depositing materials in a layer-upon-layer manner, which reduces the manufacturing considerations during the product design stage and simplify the workflow of product fabrication. 3D printed force sensors using specially developed materials can be fabricated in any form to best fit the product design requirements instead of the other way around. Furthermore, the performance of these 3D printed sensors can also be tuned by changing the material composition or the 3D printing parameters. Saari et al. [15] developed a composite 3D printed force sensor that uses the measured capacitance change to estimate the applied force on the sensor. Metal wires in a tight spiral pattern are integrated in the 3D printed frame to generate capacitance and linear response are found between the capacitance and the applied force. Liu et al. [16] designed and fabricated a resistive force sensor by combining two 3D printing technologies: Digital Light Processing (DLP) 3D printing and inkjet printing, where conductive ink is applied to offer the conductivity. The fabricated sensor can be used for both force sensing and strain measurements. Choudhary et al. [17] review the advances in 3D printed force sensors and discuss the steps to consider in design and fabricating these sensors.

However, most of the aforementioned 3D printed sensors focus on unidirectional strain or force sensing. Multi-axial force sensors that can measure the applied force in different directions are rarely discussed. To this goal, in this article we introduce a 3D printed cube-shape multi-axial force sensor. The sensor shows resistance change in different axes when external forces are applied in different directions, which is applied to estimate the external forces. The experimental setup for characterizing the resistance-force relationship of a sensor prototype is introduced. The sensor is then tested with unidirectional and bidirectional forces and its resistance changes are measured. Then, different data-driven models are acquired to represent the sensor performances in single and two directions. Finally, the model acquired for bidirectional sensing is then applied to detect haptic force manually applied as a validation case study. It is demonstrated that the strain-resistance change at different deformation directions of the 3D printed sensor can be decoupled, making the approach suitable for fabricating customized multi-axial sensors for the production industry.

The rest of this article is structured as follows: Section 2 introduces the fabrication method of the multi-axial sensor prototype and the components enabling the experiments

**Table 1.** 3D printing parameters

Parameters	Value
Layer height ( <i>mm</i> )	0.3
First layer height ( <i>mm</i> )	0.3
Extrusion width ( <i>mm</i> )	0.5
Fill	
Fill density (%)	100
Fill angle (degree) (%)	45
Speed	
Print speed ( <i>mm/s</i> )	22
First layer speed ( <i>mm/s</i> )	11
Temperature	
Extruder temperature ( $^{\circ}\text{C}$ )	235
Bed temperature ( $^{\circ}\text{C}$ )	50
Machine	
Nozzle size ( <i>mm</i> )	0.4

for characterizing the unidirectional and bidirectional performance of the printed sensor. In Section 3, the experimental results are discussed and models are built to represent the loading-resistance performances when the external loading is applied in single and two directions. Section 4 presents a case study where random forces are manually applied to two sides of the sensor and the measured forces are estimated by the models derived in Section 3, while also validated with individual commercial force sensors. Finally, concluding remarks are provided in Section 5.

## 2. Methods

### 2.1. 3D printing of the cube shape multi-axial sensor

A TL-D3 Pro Dual Extruder 3D Printer is used to print the sensors. The printer is a Fused Deposition Modeling (FDM) 3D printer provided by Shenzhen Tenlog 3D Technology Co., Ltd. It has two independent direct drive extruders that can smoothly extrude flexible materials. The NinjaTek EEL filament is used for the fabrication of the sensor. The material EEL is composed of Thermoplastic polyurethane (TPU) and carbon black, which makes the TPU conductive and its electric resistance is found to be strain responsive due to the distribution change of the carbon black during the deformation. The material is also flexible with tensile stress of 11 *MPa* at 300% elongation and can be elongated up to 355%. The sensor prototype is printed as a cube with side length of 10 *mm* and the key 3D printing parameters are shown in Table 1.

### 2.2. Loading application unit

To characterize the performance of the 3D printed sensor, variable loading is applied onto the sensor and the resistance changes are recorded. The loading is applied via 1 *mL* NORM-JECT syringes as shown in Figure 1(a), where air pressure is applied from the

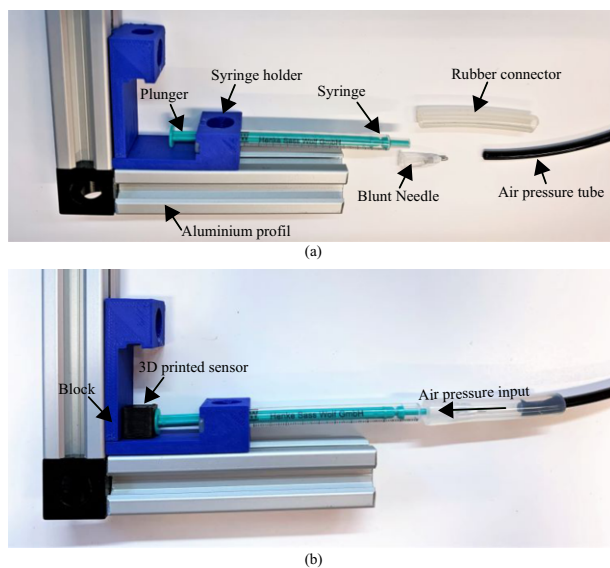


**Figure 1.** Loading supplied with pressurized syringe. (a) Parts for the loading supply unit. (b) Assembled loading supply unit.

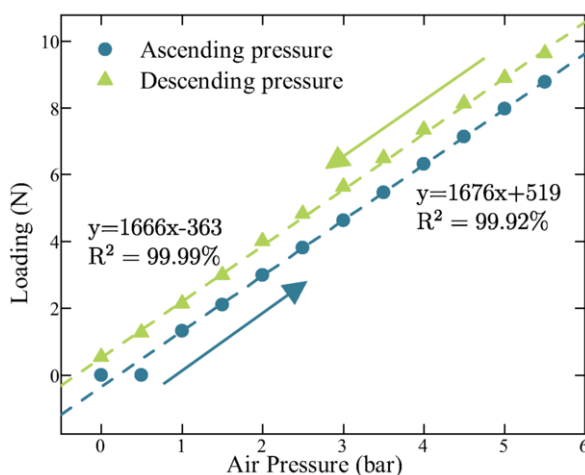


**Figure 2.** Variable sensor loading by applying different air pressures via the syringe.

outlet side of the syringes. When the barrel is pressurized, the plunger is pushed towards the opposite direction and exerts a load to the sensor as shown in Figure 1(b).

Figure 2 shows the variation of the output loading via the syringe plunger, which was recorded with an analytical balance with ascending and descending input air pressure. During pressure increase, the output pressure remains at zero until the air pressure reaches 1 bar due to the friction between the plunger and the barrel of the syringe. After that point, the loading increases linearly versus the increased pressure and the fitted linear function is shown in Figure 2. During the depressurization stage, an loading offset occurs as the plunger now moves towards the opposite direction, which causes the friction

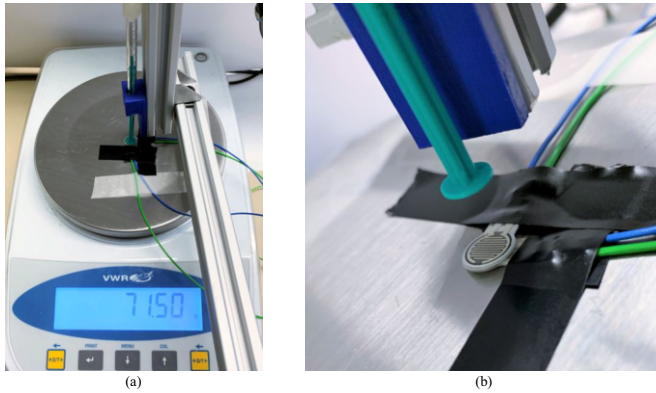


**Figure 3.** Setup for FSR calibration. (a) The loading supply unit is placed above the analytical balance. (b) The FSRs are fixed on the plate of the balance under the syringe plunger.

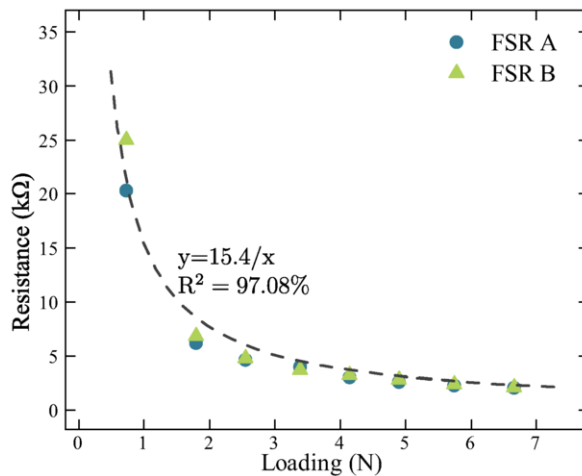


**Figure 4.** Performance of the force sensing resistor (FSR).

on the plunger to also change direction. In this case, the output loading also decreases linearly and follows the input pressure with the same slope as the pressurization stage. When the air pressure becomes returns to zero, the loading is still larger than zero due to friction. As extracted from the linear curve fittings for the data shown in Figure 2, the slopes of the two fitted lines are arithmetically close, demonstrating that the measured loading is linear to the air pressure input into the syringe. For an ideal syringe without friction, when the input air pressure is zero, the output loading is also zero. Thus, the intersections with the vertical axis of the two fitted lines shows that the influence of the friction on the output loading is around  $\pm 363 \sim 519 \text{ N}$ .

### 2.3. Load sensing with force sensing resistors

The existence of the friction force makes the output loading from the syringe unpredictable. To keep accurate recordings of the actual loading applied on the 3D printed

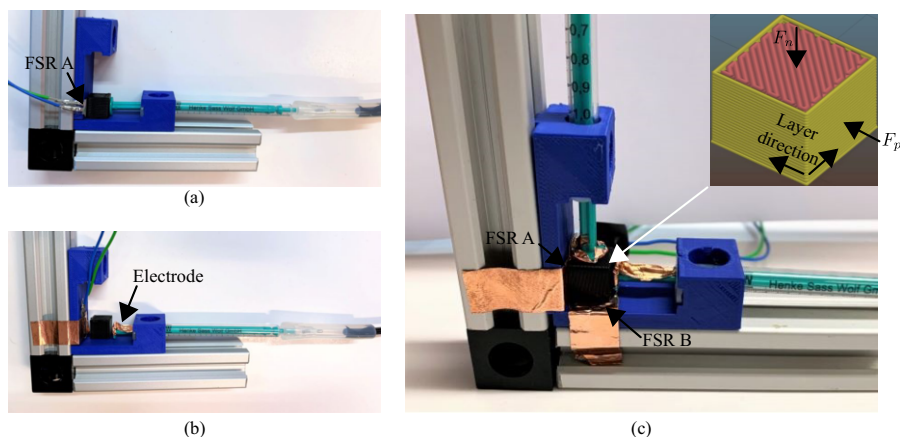


**Figure 5.** Experimental setup. (a) FSR is placed to measure the actual loading on the 3D printed sensor. (b) Electrodes are attached to the two sides of the 3D printed sensor to measure the directional resistance. (c) Electrodes for bidirectional resistance measurement.

sensor, a flexible force sensing resistor (FSR, RP-C10-ST from LRGACT co.) with a diameter of 10 mm are used. The resistance of the sensor changes when loads are applied on the surface of the sensor. Its resistance-load relation is firstly calibrated using an analytical balance as shown in Figure 4(a). The readings from the analytical balance is converted from mass to force with a gravitational acceleration of  $9.8 \text{ m/s}^2$ . The loading supply unit is placed vertically and two FSRs are fixed on top of each other to the plate of the balance via tapes so equal force are applied on the two FSRs to validate the equality of the two sensors. When the syringe is pressurized, the plunger will apply force on the FSRs.

Figure 4 shows the test data for the two FSRs, where the loading is applied with the above syringe method. It can be observed that larger loading on the FSR causes larger resistance drop. The MATLAB Curve Fitting Toolbox is applied to fit the data using a power function and it is found that the relation between the FSR resistance  $R_s$  and the loading  $F_s$  can be expressed as follows:

$$R_s = \frac{15.4}{F_s} \quad (1)$$

while the Coefficient of determination  $R^2$  score of the fitting is 95.08%. The units of  $R_s$  and  $F_s$  in Eq. (1) are  $k\Omega$  and  $N$  respectively. The measurements from both FSRs are all close to the fitted curve and are considered as equal. Thus the loading on the pressure can be estimated with its resistance as follows:

$$F_s = \frac{15.4}{R_s} \quad (2)$$

#### 2.4. Experimental setup

For testing the 3D printed force sensor performance, the above FSR is placed on one side of the 3D printed sensor in opposite to the syringe loading side, as shown in Figure 5(a).

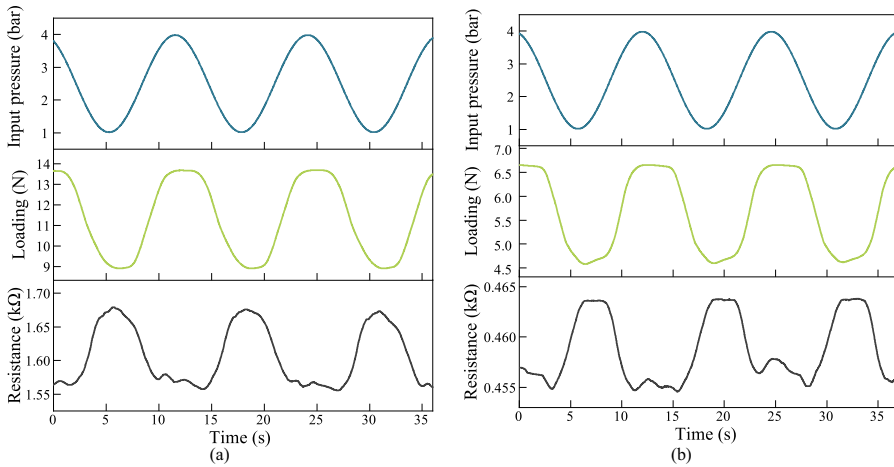


**Figure 6.** Unidirectional loading test. (a) Loading and resistance in the normal direction to the layer direction. (b) Loading and resistance in the parallel direction to the layer direction.

The real time resistance of the FSR is recorded and the corresponding force is calculated using Eq. (2), which is then considered as the loading on the 3D printed force sensor. The directional resistance of the 3D printed sensor are measured to study the loading-resistance relationship. Thus, electrodes made from copper tapes are attached to the block and the plunger of the syringe so they contact the opposite sides of the 3D printed sensor when air pressure is applied in the syringe. Figure 5(b) shows that electrodes are attached in the horizontal direction to measure the resistive uni-directional performance of the 3D printed sensor. Figure 5(c) shows the attached electrodes in two directions for measuring the bidirectional resistive performance of the 3D printed sensor, while a second FSR was added underneath the 3D printed sensor for enabling the force measurement in that second direction. Due to the anisotropy caused by the 3D printing process, the resistive properties of the printed sensor are supposed to be different at different directions. Thus, the force applied to the cube shape sensor are divided into two categories: the force normal to the layer direction is noted as  $F_n$  and the force in parallel to the layer direction is noted as  $F_p$  as illustrated in Figure 5(c).

### 3. Results

#### 3.1. Unidirectional performance of the 3D printed multi-axial sensor

Unidirectional forces are firstly applied to the direction normal to the layer direction and the direction in parallel to the layer direction as aforementioned. Periodic sine wave pressure input is applied into the syringe and the actual generated loading onto the 3D printed force sensor is acquired from the FSR placed on the other side of the respective force applying side. Figure 6(a) shows the input pressure variation with a frequency of  $0.5 \text{ rad/s}$  and an amplitude of  $3 \text{ bars}$ . The loading is applied in the normal direction to the printing layer direction. The actual loading values are also plotted in the same figure. The corresponding electric resistance of the 3D printed force sensor in the same direction is also recorded as shown in the same figure at the bottom. A periodic change in

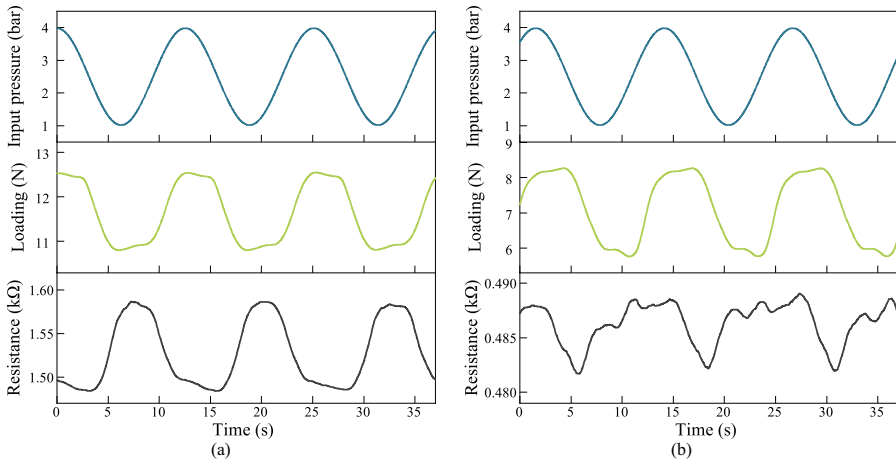


**Figure 7.** Bidirectional loading test. (a) Loading and resistance in the normal direction to the layer direction. (b) Loading and resistance in the parallel direction to the layer direction. Same sine wave input pressure is applied in the two directions simultaneously and the delay between (b) and (a) is 1/4 of the period.

resistance variation is observed, while decreasing in nature when the loading increases. The relation between the resistance and the loading is similarly fitted using the MATLAB curve fitting toolbox with a first order linear function which can be expressed as:

$$F_n^s = C_{n0}^s + C_{n1}^s R_n^s \tag{3}$$

where  $F_n^s$  is the force in the normal direction to the layer plane and  $R_n^s$  is the resistance in the same direction. The symbol  $s$  refers to the single directional force scenario. The coefficients from data fitting are:  $C_{n0}^s = 75.5$  and  $C_{n1}^s = -39.2$ . The  $R^2$  score of data fitting is 90.5%.

Same tests are performed in the direction in parallel to the layer plane and the results are shown in Figure 6(b). It can be observed that the overall generated loading in this direction is smaller than the previous direction which is resulted from the different frictions with different syringes. The overall resistance in this direction is also smaller than the direction normal to the layer plane. However, the resistance still shows periodic variation versus the loading. Same linear function is then applied to fit the resistance-loading model:

$$F_p^s = C_{p0}^s + C_{p1}^s R_p^s \tag{4}$$

where  $F_p^s$  and  $R_p^s$  are the loading and resistance in the direction in parallel to the layer direction and the coefficients are:  $C_{p0}^s = 108$ ,  $C_{p1}^s = -222.5$ ,  $R^2 = 90.5\%$ . With Eqs. (3) and (4), the applied one directional force onto the 3D printed sensor can be estimated with the measured resistance in the corresponding direction.

### 3.2. Bidirectional performance of the 3D printed multi-axial sensor

Bidirectional forces are then applied simultaneously in parallel and normal to the layer direction on the 3D printed force sensor, with the respective resistances being measured as shown in Figure 7. Similar sine wave inputs are applied as unidirectional experiments

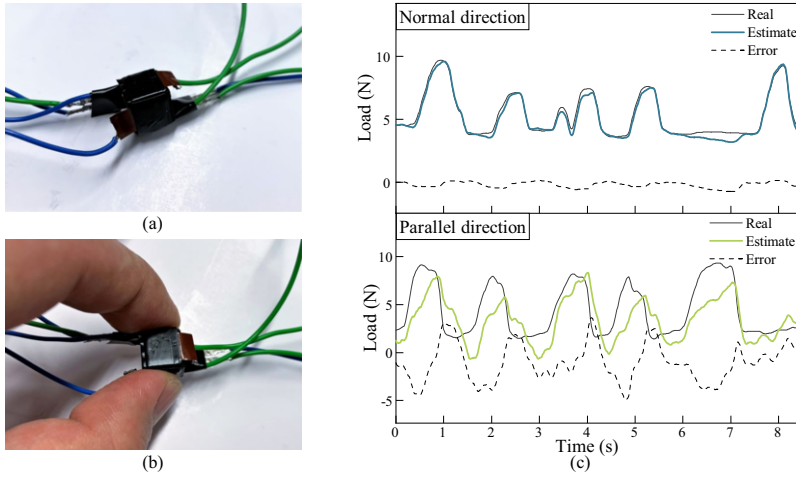


**Figure 8.** Force estimation test with manually applied haptic force on the 3D printed multi-axial force sensor. (a) Assembled force sensor. (b) Applying random haptic force on the force sensor. (c) Comparison between the estimated force and the actual force.

and a time delay of  $1/4$  of the period of the input pressure between the inputs in the two directions is applied to increase the input complexity. Two models are acquired to estimate the loading in the two directions respectively with the two resistances in the two directions as the input of the model functions. The model in the normal direction to the layer direction is:

$$F_n^b = C_{n0}^b + C_{n1}^b * R_n^b + C_{n2}^b * R_p^b \quad (5)$$

where the symbol  $b$  means bidirectional force input and the coefficients are:  $C_{n0}^b = -42.6$ ,  $C_{n1}^b = -12.3$  and  $C_{n2}^b = 150$ . The  $R^2$  score is 92%. The model in the parallel direction to the layer direction is:

$$F_p^b = C_{p0}^b + C_{p1}^b * R_n^b + C_{p2}^b * R_p^b \quad (6)$$

where  $C_{p0}^b = 187$ ,  $C_{p1}^b = -21.7$ ,  $C_{p2}^b = -302$  and the  $R^2$  score is 67%. Eqs. (5) and (6) enables the estimation of the two axial forces using the directional resistances in the bidirectional force input scenario.

#### 4. Case study: haptic force measurement with the 3D printed multi-axial sensor

The 3D printed force sensor is then assembled with the electrodes as shown in Figure 8(a). The FSRs are also integrated for validation purposes. Haptic forces are applied randomly to the normal and parallel directions to the 3D printing layer direction as shown in Figure 8(b) and the applied forces are then calculated using the resistance-force models obtained in the bidirectional testing stage.

Figure 8(c) shows the comparison between the estimated haptic force and the real load from the FSRs. The errors are also plotted in the figure. The estimation in the normal direction is accurate with errors always less than  $0.2\text{ N}$  while estimations in the par-

allel direction follow the overall trend of the actual load but the magnitude of the errors is comparable to the actual loading values, which requires further improvement of the model in the parallel direction.

## 5. Conclusion

This study introduces the design, fabrication, testing and verification of a 3D printed multi-axial force sensor. The principle of the sensor is explained and the 3D printing process is explored. A test rig enabling the unidirectional and bidirectional force loading, force recording and resistance measurement is development for characterizing the resistive properties of the 3D printed sensor in one and two directions.

Resistance-force models are built with data-driven approach for the unidirectional loading in different directions and bidirectional loading in two directions. The models are then validated in a case study where haptic forces are applied and measured by the 3D printed sensor. The study demonstrates that the strain-resistance performance of the 3D printed sensor can be decoupled via experimental measurements, thus proving that the approach can be further applied to fabricate customized sensors for different production areas.

In the future, the work will be improved in the following aspects: 1) Complex and longer time period input loading acquired for the characterization of the sensor. 2) Advanced models will be developed to represent the resistance-force relationship and better estimate the applied load. 3) Sensors of different structures will be developed to enable force sensing in more directions.

## References

- [1] Fleming WJ. Overview of automotive sensors. *IEEE sensors journal*. 2001;1(4):296-308.
- [2] Bakker E, Telting-Diaz M. Electrochemical sensors. *Analytical chemistry*. 2002;74(12):2781-800.
- [3] Husmann A, Betts J, Boebinger G, Migliori A, Rosenbaum T, Saboungi ML. Megagauss sensors. *Nature*. 2002;417(6887):421-4.
- [4] Baxter LK. Capacitive sensors. *Design and Applications*. 1997.
- [5] Xin J, Kaixuan Z, Jiangtao J, Xinwu D, Hao M, Zhaomei Q. Design and implementation of intelligent transplanting system based on photoelectric sensor and PLC. *Future Generation Computer Systems*. 2018;88:127-39.
- [6] Fericean S, Droxler R. New noncontacting inductive analog proximity and inductive linear displacement sensors for industrial automation. *IEEE Sensors Journal*. 2007;7(11):1538-45.
- [7] Byrne C, Lim CL. The ingestible telemetric body core temperature sensor: a review of validity and exercise applications. *British journal of sports medicine*. 2007;41(3):126-33.
- [8] Ji Q, Chen M, Zhao C, Zhang X, Wang XV, Wang L, et al. Feedback Control for the Precise Shape Morphing of 4D-Printed Shape Memory Polymer. *IEEE Transactions on Industrial Electronics*. 2020;68(12):12698-707.
- [9] Turner R, Fuieler PA, Newnham R, Shrout TR. Materials for high temperature acoustic and vibration sensors: A review. *Applied acoustics*. 1994;41(4):299-324.
- [10] Didosyan YS, Hauser H, Wolfmayr H, Nicolics J, Fulmek P. Magneto-optical rotational speed sensor. *Sensors and Actuators A: Physical*. 2003;106(1-3):168-71.
- [11] Muralidharan ST, Zhu R, Ji Q, Feng L, Wang XV, Wang L. A soft quadruped robot enabled by continuum actuators. In: 2021 IEEE 17th International Conference on Automation Science and Engineering (CASE). IEEE; 2021. p. 834-40.

- [12] Ji Q, Zhang X, Chen M, Wang XV, Wang L, Feng L. Design and closed loop control of a 3D printed soft actuator. In: 2020 IEEE 16th International Conference on Automation Science and Engineering (CASE). IEEE; 2020. p. 842-8.
- [13] Pierrot F, Dombre E, Dégoulange E, Urbain L, Caron P, Boudet S, et al. Hippocrate: A safe robot arm for medical applications with force feedback. *Medical Image Analysis*. 1999;3(3):285-300.
- [14] Yang H, Chen Y, Sun Y, Hao L. A novel pneumatic soft sensor for measuring contact force and curvature of a soft gripper. *Sensors and Actuators A: Physical*. 2017;266:318-27.
- [15] Saari M, Xia B, Cox B, Krueger PS, Cohen AL, Richer E. Fabrication and analysis of a composite 3D printed capacitive force sensor. *3D Printing and Additive Manufacturing*. 2016;3(3):136-41.
- [16] Liu M, Zhang Q, Shao Y, Liu C, Zhao Y. Research of a novel 3D printed strain gauge type force sensor. *Micromachines*. 2019;10(1):20.
- [17] Choudhary H, Vaithyanathan D, Kumar H. A Review on 3D printed force sensors. In: *IOP Conference Series: Materials Science and Engineering*. vol. 1104. IOP Publishing; 2021. p. 012013.